Synthesis and Electrochemical Performance of plate-like structure $LiMn_{0.8}Fe_{0.2}PO_4$/C as a Cathode Material for Lithium Ion Battery

Jun-Wei XIONG[1,a], Yuan-Zhong WANG[2,b], Ying-Ying WANG[2,c] and Jian-Xin ZHANG[1,d *]

[1] Key Laboratory for Liquid-Solid Structural Evolution & Processing of Materials (Ministry of Education), Shandong University, Jinan 250061, China

[2] Research Institute of Technology, Shandong WINA Green Power Technology Co., Ltd., Weifang 262700, China

[a]xiongjw97@163.com, [b]wangyuanzhong8500@163.com, [c]yywang0315@163.com, [d]jianxin@sdu.edu.cn

*Corresponding author

Keywords: Lithium iron manganese phosphate, Plate-like structure, Electrochemical performance, Lithium ion battery.

Abstract. Olivine plate-like structure $LiMn_{0.8}Fe_{0.2}PO_4$/C has been successfully synthesized under mild conditions using H_2O/DMSO as solvent and CTAB as surfactant. DMSO and CTAB promote the formation of plate-like structure. The prepared plate-like structure $LiMn_{0.8}Fe_{0.2}PO_4$/C delivers a reversible capacity of 141mAh·g^{-1} at 0.1C-rate, with 80.2% capacity retention at 7C-rate. Meanwhile, the plate-like structure $LiMn_{0.8}Fe_{0.2}PO_4$/C exhibits excellent cycling stability at room temperature with 98.8% capacity retention after 60 cycles at 1C-rate. The plate-like structure $LiMn_{0.8}Fe_{0.2}PO_4$/C cathode materials may have a promising potential application in li-ion batteries.

Introduction

The olivine-structured lithium transition metal ($LiMPO_4$, M=Mn, Fe, Ni, Co) as a cathode materials for lithium ion batteries has been attracted increasing attention because of its high theoretical capacity, low cost, potential electrochemical property, thermal stability and environmental friendliness [1]. These $LiMPO_4$ materials have the ability to restrict the internal short circuit in lithium ion battery, because the open phosphate structure of $LiMPO_4$ can promote the motion of lithium ions and the strong covalent P-O bond energy contributes to avoid the oxygen loss and enhance the structure stability [2,3].

The $LiMn_{1-x}Fe_xPO_4$ solid solution cathode materials with high potential(~4.1V) and improved ionic and electronic conductivities are becoming present research focuses. Up to now, considerable studies have been conducted on $LiMn_{1-x}Fe_xPO_4$, with an emphasis on the synthetic methods to control the morphology and improve the electrochemical performance. Various morphologies such as nanoparticles [4-7], nanorods [8], nanoplates [9,10], microspheres [1,11,12] and hollow spheres [13,14] have been synthesized for the $LiMn_{1-x}Fe_xPO_4$. The structure superiorities of different morphologies have been used to improve lithium ion storage properties compared with the bulk counterparts. However, all these synthetic methods for various morphologies demonstrate their deficiencies, such as complicated synthetic process, high cost for large-scale production and high time-energy consumption. Exploring a simple, reliable and less chemical intensive techniques still face large challenges. To use porous material owning high electrode-electrolyte effective contact area, short diffusion path for Li^+ transport and good volume strain accommodate as the cathode of lithium-ion batteries is one possible strategy to enhance the rate performance and cycling life of electrode materials.

Herein, we synthesized plate-like structure $LiMn_{0.8}Fe_{0.2}PO_4$/C using a facile and energy-saving oil bath method under relative low temperature(130°C) and normal pressure followed with further annealing process. The dimethylsulfoxide (DMSO) was used to raise the boiling point of hybrid reactants and reduce the Gibbs Free Energy for the reaction. Cetyl Trimethyl Ammonium Bromide (CTAB) serves as surfactant. The synergy of DMSO and CTAB promoted the formation of

plate-like structure. Moreover, plate-like structure $LiMn_{0.8}Fe_{0.2}PO_4/C$, as electrodes, show excellent rate capability and cycle stability.

Experimental Section

Materials Synthesis

Plate-like structure $LiMn_{0.8}Fe_{0.2}PO_4/C$ was synthesized with oil bath method using H_2O/DMSO as solvent and CTAB as surfactant.

Firstly, according to the stoichiometry, a certain amount of $MnSO_4·H_2O$, $FeSO_4·7H_2O$ and $(NH_4)H_2PO_4$ were dissolved in a certain volume of distilled water in sequence to form 0.8M $MnSO_4·H_2O$, 0.2M $FeSO_4·7H_2O$ and 1M $(NH_4)H_2PO_4$ aqueous solutions. Secondly, the same volume of DMSO was added to the solution. 0.5g CTAB was added into the above mixture with magnetically stirring for about 1h. Afterward, 3M $LiOH·H_2O$ was added into the above solution slowly with continuous stirring for about 2h. A spot of ammonium hydroxide was added dropwise into the mixture to adjust the pH of 10. The mixture was heated in an oil bath at 130°C for 6 h under argon atmosphere. After the solution was cooled to room temperature, the solid precipitate was washed for several times with deionized water and absolute ethanol, and finally dried in a vacuum drying oven at 80°C for 10h, then sieved to obtain $LiMn_{0.8}Fe_{0.2}PO_4$ sample. For comparison, $LiMn_{0.8}Fe_{0.2}PO_4$ sample without CTAB was also synthesized via the same procedures.

In order to obtain a uniform carbon coating on the surfaces of the $LiMn_{0.8}Fe_{0.2}PO_4$ products, they were mixed with sucrose in a weight ratio of 10:1. The mixture was pre-sintered at 250°C for 2h and subsequently calcined at 600°C for 10h under dynamic argon atmosphere with a heating rate of $10°C·min^{-1}$. After cooling down to room temperature, the $LiMn_{0.8}Fe_{0.2}PO_4/C$ materials were obtained.

Material Characterization

The crystal phases of as-prepared samples were characterized by X-Ray Diffraction (XRD) using a Rigaku Dmax-rc diffractometer with Cu Kα radiation (λ=0.154nm), and the morphologies were observed by field emission scanning electron microscopy (FESEM, Hitachi SU-70, Japan) and high resolution transmission electron microscopy (HRTEM, JEM-2100, 200 kV, Japan). The Brunauer-Emmett-Teller (BET) surface area and pore size distribution were performed by ASAP 2020 V3.01 G system.

Electrochemical Performance Tests

Electrochemical measurements were carried out using CR2025 coin-type cells with lithium foil as the counter and reference electrodes. The working electrodes was mixed by dispersing the sample powders, acetylene black and polyvinylidene fluoride(PVDF) in a weight of 8:1:1 in N-methyl-2-pyrrolidone (NMP). The mixture was magnetic stirred for 24h. Then the acquired slurry was coated uniformly on aluminum foil and dried under a vacuum at 120°C overnight. The electrode was cut into a circle shape with diameter of 14mm for a cell. The cells were assembled in an Ar-filled glove box (SG2400/750TS, Vigor). The electrolyte solution was 1 $mol·L^{-1}$ $LiPF_6$ dissolved in ethylene carbonate (EC) and dimethyl carbonate (DMC) and diethyl carbonate (DEC) with the volume ratio of 3:1:1. The electrochemical performances of the samples were measured by galvanostatic cycling between 2.5V and 4.5V on a multi-channel battery testing instrument (LAND CT2001A) at various current densities (1C=170$mA·g^{-1}$). For the as-prepared materials, the electrochemical impedance spectroscopy (EIS) within 10-100KHz was performed by Advanced Electrochemical System (Ametek PARSTAT 2273).

Results and Discussion

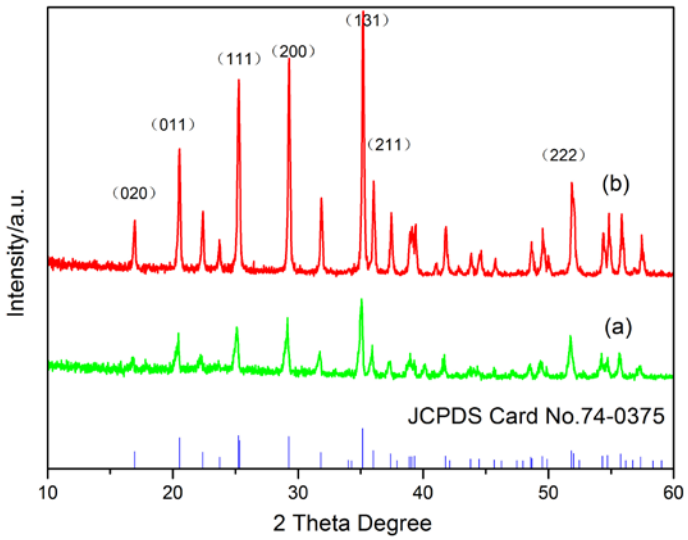

Fig. 1. XRD patterns of the prepared plate-like structure $LiMn_{0.8}Fe_{0.2}PO_4/C$(a) and $LiMn_{0.8}Fe_{0.2}PO_4/C$ nanoparticles(b).

Fig.1 shows the XRD patterns of the plate-like structure $LiMn_{0.8}Fe_{0.2}PO_4/C$ and $LiMn_{0.8}Fe_{0.2}PO_4/C$ nanoparticles. As shown in Fig.1a, the plate-like structure $LiMn_{0.8}Fe_{0.2}PO_4/C$ is almost pure-phase olivine structure indexed to orthorhombic (Pmnb space group) when compared to the standard PDF card (JCPDS 74-0375). Fig.1b shows the XRD patterns of $LiMn_{0.8}Fe_{0.2}PO_4/C$ nanoparticles, all peaks can be well indexed to a single phase olivine type orthorhombic structure with a Pnmb space group (JCPDS 74-0375). No peaks of impurity phases were found in the two samples. Moreover, no obvious praks of carbon was observed, which is attributes to the amorphous nature of the residual carbon layers and the low content. It is worthy to note that $LiMn_{0.8}Fe_{0.2}PO_4/C$ samples are directly obtained by heating with oil bath under low temperature and ambient pressure. This indicates that this method is simple, low requirement on environment and easy to realize the industrialization.

The morphologies of $LiMn_{0.8}Fe_{0.2}PO_4$ and $LiMn_{0.8}Fe_{0.2}PO_4/C$ samples were examined by FESEM and HRTEM. As shown in Fig.2a, the $LiMn_{0.8}Fe_{0.2}PO_4$ nanoparticles are irregular spheres with the size of 500nm in diameter. The particles are obviously agglomerated and the surface of particles is rough. Fig.2b exhibits a platelike morphology, the diameter of the plates is about 10-20μm. It can be clearly seen that the thickness of plate-like structure $LiMn_{0.8}Fe_{0.2}PO_4$ is nanoscale. Thin plate-like structure is beneficial to the fast migration of Li^+ between the plates. This can also increase the ionic conductivity. The HRTEM image in Fig.2c suggests that plate-like structure $LiMn_{0.8}Fe_{0.2}PO_4$ is coated by uniform carbon layer with about 3.54nm thick. As reflected by an irregular strip, the carbon layer can facilitate the construction of the conducting network. Therefore, electron transference in the electrode materials will become even easier, and electrochemical performance will be improved. The HRTEM image also shows a regular fingerprint, indicating a highly crystallinized phase in the cores of each plates. The lattice fringes with a width of 0.357nm correspond to the d-spacing of the (111) crystal planes of a typical $LiMn_{0.8}Fe_{0.2}PO_4$ crystal [3].

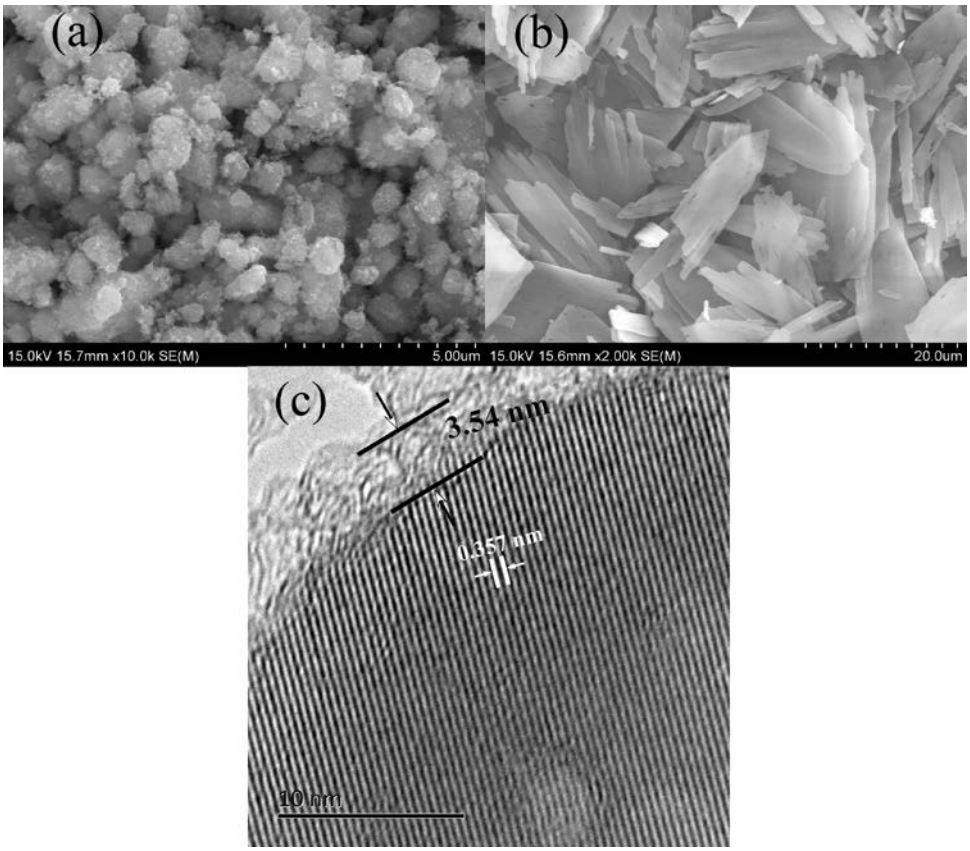

Fig.2. SEM images of $LiMn_{0.8}Fe_{0.2}PO_4$ nanopaticles (a) and plate-like structure $LiMn_{0.8}Fe_{0.2}PO_4$ (b); HRTEM image of plate-like structure $LiMn_{0.8}Fe_{0.2}PO_4$/C(c).

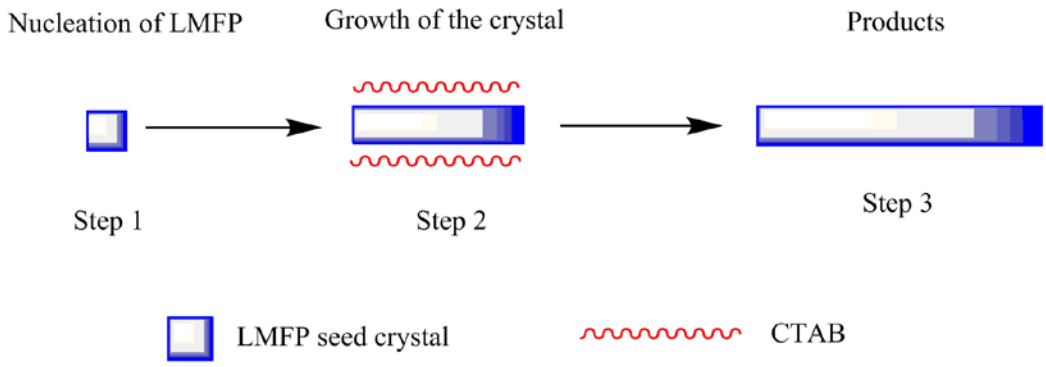

Fig.3. The formation process of plate-like structure $LiMn_{0.8}Fe_{0.2}PO_4$.

CTAB as a surfactant plays an important role in directing the crystal face growth along certain direction to form unique structure [15]. Fig.3 describes the formation process and the influence of surfactant during the formation process of plate-like structure $LiMn_{0.8}Fe_{0.2}PO_4$. In the process of reaction, the nucleation center is first formed, then the nucleation is covered by CTAB, CTAB reduces the surface energy of certain crystals and suppresses the growth of specific faces of crystal, while other faces with high surface energy fast grow. As the reaction, $LiMn_{0.8}Fe_{0.2}PO_4$ grows into the highly ordered plate architectures.

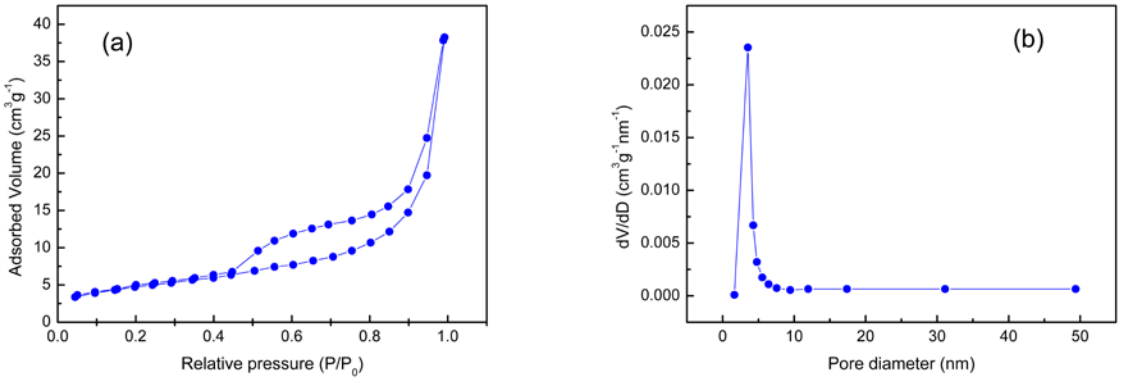

Fig.4. Nitrogen adsorption and desorption isotherms (a) and the corresponding pore-size distribution calculated by BJH method from the desorption branch (b) of plate-like structure $LiMn_{0.8}Fe_{0.2}PO_4$.

As shown in Fig.4, plate-like structure $LiMn_{0.8}Fe_{0.2}PO_4$ exhibits a typical type IV isotherm with a H -type hysteresis loop, which indicating a mesoporous structure. The $LiMn_{0.8}Fe_{0.2}PO_4$ plates exhibit a Brunauer-Emmett-Teller surface area of 42.04$m^2 \cdot g^{-1}$. The meanly pore size distribution was 3.954nm, which confirms the porous structure. These pores might be formed due to the decomposition of sucrose in sintering process. During the process, sucrose melts and decomposes at lower temperature to form caramel first, and then carbonizes at a higher temperature with generating CO_2, CO and H_2O, which are responsible for the formation of pores in the plate-like structure $LiMn_{0.8}Fe_{0.2}PO_4$[11].

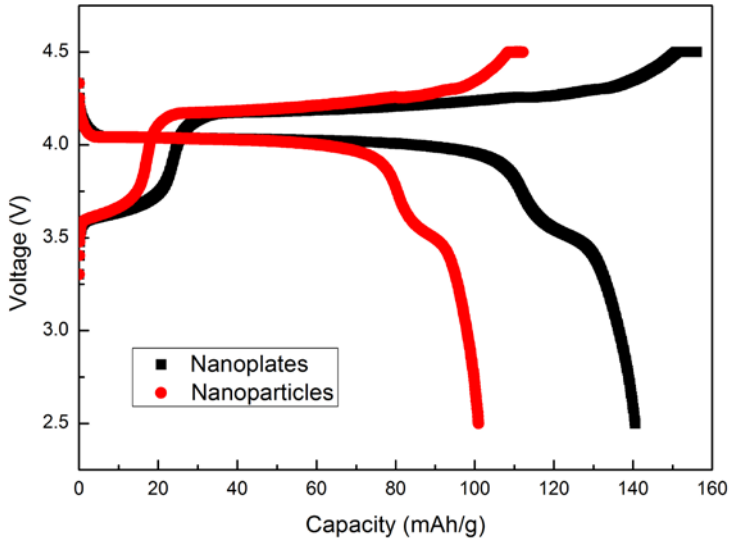

Fig.5. Initial charge-discharge curves (0.1C) of plate-like structure $LiMn_{0.8}Fe_{0.2}PO_4$ and $LiMn_{0.8}Fe_{0.2}PO_4$ nanopaticles.

The potential applications of plate-like structure $LiMn_{0.8}Fe_{0.2}PO_4$ and $LiMn_{0.8}Fe_{0.2}PO_4$ nanopaticles in lithium ion batteries were investigated by assembling them into CR2025 cells. The cells were charged to 4.5V at 0.1C, and maintained at 4.5V until the limited current 0.02C was reached, and then discharged to 2.5V at 0.1 C (1C equal to 170mA/g). As can be seen from Fig.5, the initial charge/discharge curves contain two couples of platforms at approximately 3.5 and 4.1V, associated with the Fe^{3+}/Fe^{2+} and Mn^{3+}/Mn^{2+} redox couples, respectively. Although two samples show similar charge and discharge profiles, it is clear that the plate-like structure $LiMn_{0.8}Fe_{0.2}PO_4$

sample showed a much higher reversible capacity compared to the $LiMn_{0.8}Fe_{0.2}PO_4$ nanopaticles. Charge and discharge specific capacities at 0.1C were 156.1mAh/g and 140.5mAh/g for the plate-like structure $LiMn_{0.8}Fe_{0.2}PO_4$, which correspond to a coulombic efficiency of 90.0%. While the charge and discharge specific capacities at 0.1C were 113.2mAh/g and 99.8mAh/g for the $LiMn_{0.8}Fe_{0.2}PO_4$ nanopaticles, which correspond to a coulombic efficiency of 88.0%. Although two samples exhibited high coulomb efficiency, the tiny irreversible capacity mainly attribute to undesired side reactions caused by the poor thermal stability and the electrolyte decomposition at high voltage [16].

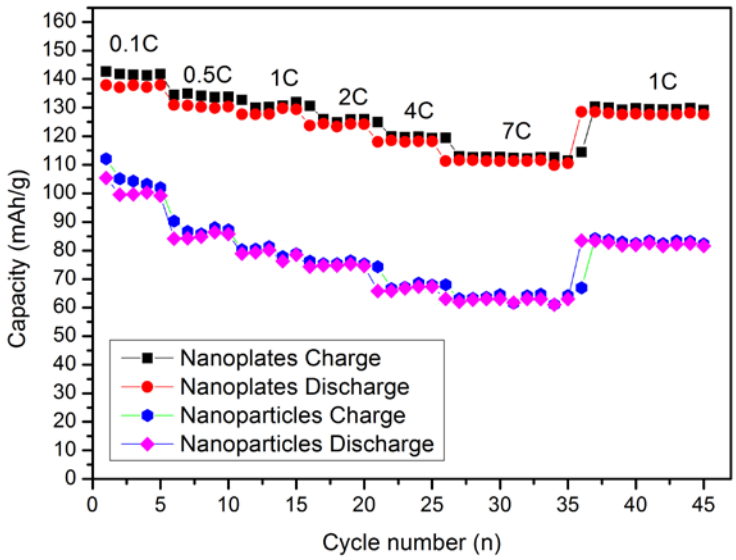

Fig.6. Rate capabilities of plate-like structure $LiMn_{0.8}Fe_{0.2}PO_4$ and $LiMn_{0.8}Fe_{0.2}PO_4$ nanopaticles.

The rate capabilities of plate-like structure $LiMn_{0.8}Fe_{0.2}PO_4$ and $LiMn_{0.8}Fe_{0.2}PO_4$ nanopaticles materials with 0.1 C, 0.5 C, 1C, 2C, 4C and 7C current densities are shown in Fig.6. The plate-like structure $LiMn_{0.8}Fe_{0.2}PO_4$ cathode materials had better rate capability than the $LiMn_{0.8}Fe_{0.2}PO_4$ nanopaticles under all charge-discharge rates. Discharge capacities of the plate-like structure $LiMn_{0.8}Fe_{0.2}PO_4$ measured at various rates are about 141, 134, 130, 126, 120, 113 $mAh \cdot g^{-1}$ at 0.1C, 0.5C, 1C, 2C, 5C and 7C, respectively. While discharge capacities of the $LiMn_{0.8}Fe_{0.2}PO_4$ nanopaticles measured at various rates are about 105, 88, 79, 76, 68, 63 $mAh \cdot g^{-1}$ at 0.1C, 0.5C, 1C, 2C, 5C and 7C, respectively. The capacity at the rate of 7C of the plate-like structure $LiMn_{0.8}Fe_{0.2}PO_4$ sample can reach 80.2% of the initial capacity at 0.1C while there is only 60.0% for $LiMn_{0.8}Fe_{0.2}PO_4$ nanopaticles. When the current rate reverts back to 1C after cycling at high rates, the original value can be recovered, which demonstrates that the two samples own good tolerance to varied current density. In contrast, the plate-like structure $LiMn_{0.8}Fe_{0.2}PO_4$ show much better rate performance than $LiMn_{0.8}Fe_{0.2}PO_4$ nanopaticles, because more serious capacity fading occurred at high rates for $LiMn_{0.8}Fe_{0.2}PO_4$ nanopaticles cells.

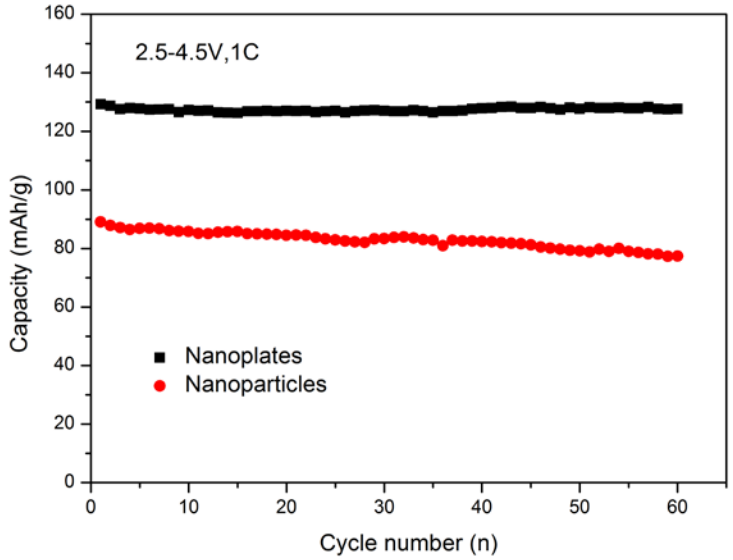

Fig.7. Cycling performances of plate-like structure $LiMn_{0.8}Fe_{0.2}PO_4$ and $LiMn_{0.8}Fe_{0.2}PO_4$ nanopaticles at 1C in the voltage range of 2.5-4.5V.

As shown in Fig.7, the reversible capacity of plate-like structure $LiMn_{0.8}Fe_{0.2}PO_4$ in the first cycle at 1C is about 129.3mAh·g^{-1}, and it exhibited the capacity retention of 98.8% and only tiny capacity loss was observed after 60 cycles. However, the $LiMn_{0.8}Fe_{0.2}PO_4$ nanopaticles has a reversible capacity about 89.1mAh·g^{-1} in the initial cycle and only 86.8% of initial capacity was retained after 60 cycles. The good cycle stability of plate-like structure $LiMn_{0.8}Fe_{0.2}PO_4$ is attributed to the short lithium ion diffusion path and porosity[17].

Summary

olivine plate-like structure $LiMn_{0.8}Fe_{0.2}PO_4$ was obtained by using a facile oil bath method under relative low temperature and normal pressure followed with further annealing process. The activation of CTAB promotes the formation of plate-like structure. The plate-like structure $LiMn_{0.8}Fe_{0.2}PO_4$ show much better rate performance and cycle stability than the $LiMn_{0.8}Fe_{0.2}PO_4$ nanopaticles. The plate-like structure $LiMn_{0.8}Fe_{0.2}PO_4$ sample exhibits a high discharge capacity of 141mAh·g^{-1} at 0.1C, and the capacity at the rate of 7C can reach 80.2% of the initial capacity. The capacity retention of 98.8% was achieved after 60 cycles at 1C. The excellent electrochemical properties are attributed to the the short lithium ion diffusion path and porosity which could enhance the ionic conductivity. Moreover, the preparation method is simple, economy and fast compared with the traditional solid state method and solvothermal method.

Acknowledgments

This work was supported by Shandong Provincial Independent Innovation and Achievement Transformation Special Funds (No. 2014ZZCX05501).

References

[1] M.S. Kim, J.P. Jegal, K.C. Roh and K.B. Kim, J. Mater. Chem. A 2 (2014) 10607-10613.

[2] P.R. Kumar, M. Venkateswarlu, M. Misra, A.K. Mohanty and N. Satyanarayana, J. Electrochem. Soc. 158 (2011) A227-A230.

[3] L.G. Wang, P.G. Zuo, G.P. Yin, Y.L. Ma, X.Q. Cheng, C.Y. Du and Y.Z. Gao, J. Mater. Chem. A 3

(2015) 1569-1579.

[4] X. Zhou, Y. Xie, Y.F. Deng, X.S. Qin and G.H. Chen, J. Mater. Chem. A 3 (2015) 996-1004.

[5] W.C. Yang, Y.J. Bi, Y.P. Qin, Y. Liu, X.H. Zhang, B.C. Yang, Q. Wu, D.Y. Wang and S.Q. Shi, J. Power Sources 275 (2015) 85-791.

[6] X.H. Yang, Y.Y. Mi, W.D. Zhang and H.H. Zhou, J. Power Sources 275 (2015) 823-830.

[7] E.R. Dai, W.B. Chen, H.S. Fang, H. Wang and W.H. Ma, EPD Congress (2015) 315-322.

[8] L.J. Hu, B. Qiu, Y.G. Xia, Z.H. Qin, L.F. Qin, X.F. Zhou and Z.P. Liu, J. Power Sources 248 (2014) 246-252.

[9] S. Wi, J. Kim, S. Nam, J. Kang, S. Lee, H. Woo, M. Lee, C.H. Sonu, T. Moon and B. Park, Curr. Appl. Phys. 14 (2014) 725-730.

[10] A. Paolella, G. Bertoni, E. Dilena, S. Marras, A. Ansaldo, L. Manna and C. George, Nano. Lett. 14 (2014) 1477-1483.

[11] Y.Y. Mi, P. Gao, W. Liu, W.D. Zhang and H.H. Zhou, J. Power Sources 267 (2014) 459-468.

[12] T. Liu, J.J. Xu, B.B. Wu, Q.B. Xia and X.D. Wu, RSC Adv. 3 (2013) 13337-13341.

[13] C.C. Xu, L. Li, F.Y. Qiu, C.H. An, Y.N. Xu, Y. Wang, Y.J. Wang, L.F. Jiao and H.T. Yuan, J. Nat. Gas Chem. 23 (2014) 397-402.

[14] Y. Lu, Z.Y. Wen, J. Jin, K. Rui and X.W. Wu, Phys. Chem. Chem. Phys. 16 (2014) 8556-8562.

[15] H. Uchiyama and H. Imai, Cryst. Growth Des. 2010, 10 (2010) 1777-1781.

[16] Y.J. Zhong, Z.G. Wu, J.T. Li, W. Xiang, X.D. Guo, B.H. Zhong and S.G. Sun, ChemElectro Chem 2 (2015) 896-902.

[17] Y. Jiang, R.Z. Liu, W.W. Xu, Z. Jiao, M.H. Wu, Y.L. Chu, L. Su, H. Cao, M. Hou and B. Zhao, J. Mater. Res. 28 (2013) 2584-2589.